sustainability

MDPI

Article

Optimal Sizing and Power System Control of Hybrid Solar PV-Biogas Generator with Energy Storage System Power Plant

Takele Ferede Agajie [1,2,*], Armand Fopah-Lele [3,*], Ahmed Ali [4], Isaac Amoussou [1], Baseem Khan [5,6], Mahmoud Elsisi [7,8], Om Prakash Mahela [6,9], Roberto Marcelo Álvarez [6,10] and Emmanuel Tanyi [1]

1 Department of Electrical and Electronic Engineering, Faculty of Engineering and Technology, University of Buea, Buea P.O. Box 63, Cameroon
2 Department of Electrical and Computer Engineering, Debre Markos University, Debre Markos P.O. Box 269, Ethiopia
3 Department of Mechanical Engineering, Faculty of Engineering and Technology, University of Buea, Buea P.O. Box 63, Cameroon
4 Department of Electrical and Engineering Technology, University of Johannesburg, Johannesburg 2006, South Africa
5 Department of Electrical and Computer Engineering, Hawassa University, Hawassa 1530, Ethiopia
6 Department of Project Management, Universidad Internacional Iberoamericana, Campeche 24560, Mexico
7 Department of Electrical Engineering, National Kaohsiung University of Science and Technology, Kaohsiung City 807618, Taiwan
8 Electrical Engineering Department, Faculty of Engineering at Shoubra, Benha University, Cairo 11629, Egypt
9 Power System Planning Division, Rajasthan Rajya Vidyut Prasaran Nigam Limited, Jaipur 302005, India
10 Higher Polytechnic School, Universidad Europea del Atlántico, C/Isabel Torres 21, 39011 Santander, Spain
* Correspondence: tferede19@gmail.com (T.F.A.); a.fopah-lele@ubuea.cm (A.F.-L.)

Abstract: In this paper, the electrical parameters of a hybrid power system made of hybrid renewable energy sources (HRES) generation are primarily discussed. The main components of HRES with energy storage (ES) systems are the resources coordinated with multiple photovoltaic (PV) cell units, a biogas generator, and multiple ES systems, including superconducting magnetic energy storage (SMES) and pumped hydro energy storage (PHES). The performance characteristics of the HRES are determined by the constant power generation from various sources, as well as the shifting load perturbations. Constant power generation from a variety of sources, as well as shifting load perturbations, dictate the HRES's performance characteristics. As a result of the fluctuating load demand, there will be steady generation but also fluctuating frequency and power. A suitable control strategy is therefore needed to overcome the frequency and power deviations under the aforementioned load demand and generation conditions. An integration in the environment of fractional order (FO) calculus for proportion-al-integral-derivative (PID) controllers and fuzzy controllers, referred to as FO-Fuzzy-PID controllers, tuned with the opposition-based whale optimization algorithm (OWOA), and compared with QOHSA, TBLOA, and PSO has been proposed to control the frequency deviation and power deviations in each power generation unites. The results of the frequency deviation obtained by using FO-fuzzy-PID controllers with OWOA tuned are 1.05%, 2.01%, and 2.73% lower than when QOHSA, TBLOA, and PSO have been used to tune, respectively. Through this analysis, the algorithm's efficiency is determined. Sensitivity studies are also carried out to demonstrate the robustness of the technique under consideration in relation to changes in the sizes of the HRES and ES system parameters.

Keywords: solar PV; energy storage system; hybrid renewable energy sources; superconducting magnetic energy storage

Citation: Agajie, T.F.; Fopah-Lele, A.; Ali, A.; Amoussou, I.; Khan, B.; Elsisi, M.; Mahela, O.P.; Álvarez, R.M.; Tanyi, E. Optimal Sizing and Power System Control of Hybrid Solar PV-Biogas Generator with Energy Storage System Power Plant. *Sustainability* **2023**, *15*, 5739. https://doi.org/10.3390/su15075739

Academic Editor: Luca Cioccolanti

Received: 28 January 2023
Revised: 16 March 2023
Accepted: 20 March 2023
Published: 24 March 2023

1. Introduction

Energy is one of the industries that is growing the fastest because it has to deal with a number of problems, such as traditional energy sources running out, global warming getting worse, and other problems. Because of these problems, it is more important

than ever to use non-traditional or renewable energy sources, such as solar, wind, and biogas [1,2]. There are a lot of these resources, but they are very random because they depend on the weather at any given time. There may be occasions when the sources' generation is not enough to satisfy the load demand at a particular moment in time. Batteries, ultra-capacitors, and flywheels might all be connected to hybrid power systems to correct this imbalance. These devices improve the quality of electricity while also lowering grid frequency variations [3,4].

Surplus power is available when the generation exceeds the load requirements, which most often occurs during peak weather conditions. At this time, storage devices temporarily store energy. This stored energy is used when the generated energy falls short of the rise in load demand. In the coming years, there will be a greater use of renewable energy sources, such as superconducting magnetic and pumped hydro energy storage systems, to reduce fuel prices, reduce CO_2 emissions, and improve network power quality [5–7]. The load frequency control scale can be used to fix imbalances caused by changes in frequency caused by the fact that wind and solar energy are not always available [8,9]. In a standby reserve, extra power is saved and can be used when the demand on the grid changes. The SMES, which are incorporated in the hybrid power system renewable energy generation analysis, have the same purpose of regulating the grid's variation in load as they are plugged in. Control strategies for coordination are required for proper performance. In [10], general classical controllers are utilized. The authors of [11] proposed the evolutionary optimization technique for a comparative analysis of various conventional controllers for an isolated wind–diesel hybrid power plant. In [12], the authors proposed employing linear matrix inequalities-based robust controller design and particle swarm optimization to manage frequency in hybrid power systems. The authors of [13] employed particle swarm optimization to control and simulate a wind–biomass isolated hybrid power system. For frequency regulation of hybrid power systems with electric vehicles, the authors in [14] developed the fractional-order adaptive fuzzy PID controller with modified salp swarm algorithm optimization. The fractional order fuzzy PID controller for frequency regulation of a solar–wind integrated power system with a hydrogen aqua equalizer-fuel cell unit was presented by the authors in [15]. In [16], the authors suggested developing a fuzzy logic controller for load frequency management in an isolated hybrid power system. A type 2 fuzzy PID controller for frequency control in hybrid distributed power systems was presented by the authors in [17]. A model of an island hybrid power system that uses artificial bee colony optimization for fuzzy logic-based load frequency management was described by the authors in [18]. The authors in [19] suggested a novel scaling factor-based fuzzy logic controller for frequency regulation of an isolated hybrid power system. The authors of [10] provided integrated frequency and power regulation of a freestanding hybrid power system while considering a fuzzy classical controller with a scaling factor. The authors of [20] described frequency control on a remote island using parallel battery systems and the H control theory based on droop characteristics. The authors of [21] introduced the dependable H-infinity load frequency control in a hybrid distributed generating system. By incorporating SVC into power system networks, the writers in [22] explained how to employ the best load flow technique in MATLAB/Simulink settings to enhance voltage profiles. Reference [23] examined the best location for static VAr compensators in electric power systems. The authors discussed the integration of static variables to account for hybrid power systems and renewable-energy-producing systems in [24].

Fractional calculus [25,26] has been used in control systems and other domains in recent years. Modern contributions to this field include control systems that use computational intelligence [27] with arbitrary time delays, such as process control [28], reactive power control [29], a cascade fuzzy-fraction order (FO)-proportional-integral-derivative (PID) controller for automated generation control (AGC) [30], and using an FO-PID with a filter for AGC in linked thermal and thermal-hydro-gas power systems [31]. In addition, ultra-capacitor effects on AGC in multi-area integrated thermal and thermal- hydro-gas power systems by utilizing a fuzzy-FO-integral-derivative controller and a PID with a filter [32], are

recent. In integrated PV, thermal, and hydrothermal power plants, load frequency control (LFC) with fuzzy FO-integral-derivative with filter [33], fuzzy PID-filter-(1 + PI) controller in AGC PV, thermal, and hydrothermal power plants [34], and others. In this paper, commonly used implementations of traditional PID, fuzzy PID, FO-PID, and FO-fuzzy PID controllers are used to show the benefits of the FO-fuzzy PID controller system.

As already discussed, solar energy is mostly intermittent, this means that the frequency of both the proposed hybrid system and the country's grid is always changing. Installing a controller with a power loop, sends or receives signals to or from the grid to energy storage devices to store or release extra or not enough power, affects the power quality. The controller may even instruct the biogas generator to transfer unusually large bursts of electricity into the national grid in order to prevent the failure of the load to which it is connected. Even better, the suggested control architecture puts all of the hybrid power system's renewable energy production under a single set of rules. Centralization also removes the need for a separate controller and tuning for power storage devices. The study area is illustrated as shown in Figure 1 by using quantum geographic information system software (qgis software version 3.8).

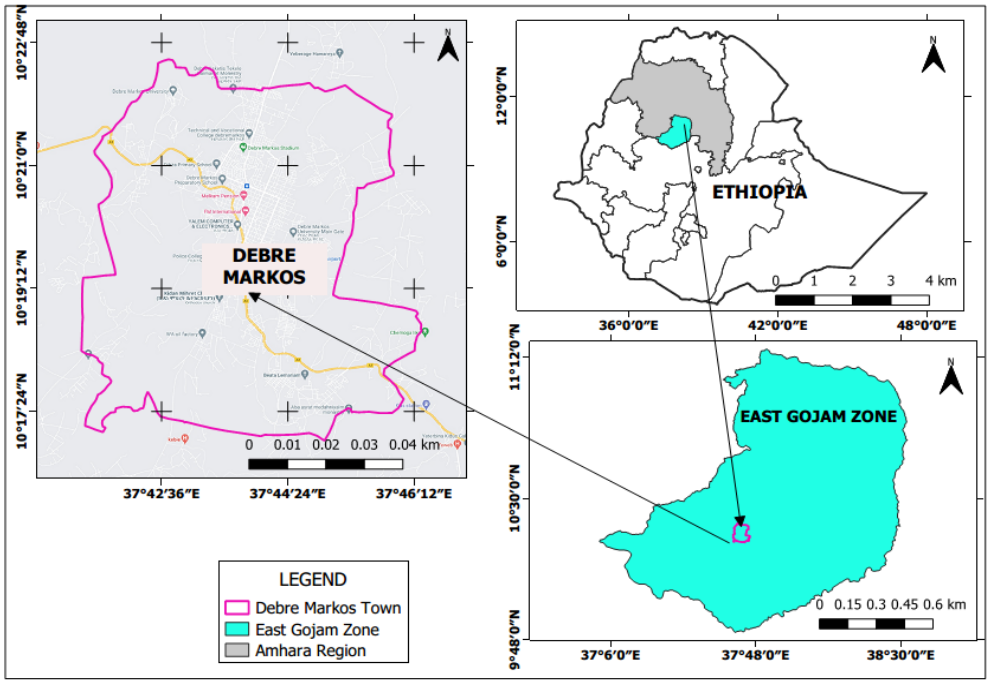

Figure 1. Map of the study area.

The present study proposes an opposition-based improved whale optimization algorithm (WOA), also known as an opposition-based along whale optimization algorithm. In comparison to other meta-heuristic algorithms, WOA is a genuine parameter optimization approach that does not use derivatives and has fewer mathematical requirements for compression. The approach could also be used to figure out how big hybrid renewable-energy-generating systems should be devised, whether connected to the grid or not. This is just one of many engineering optimization problems that the approach could help with.

The WOA metaheuristic optimization method does a better job of quickly finding high-performance zones in single and multi-objective functions cases in hybrid renewable energy sources [35]. Banerjee et al. [36] used a different method based on the HS algorithm to change the reactive power in a model of an autonomous hybrid power system. To improve performance, a new fractional order (FO) fuzzy control method is used, and its parameters are changed with the help of a particle swarm optimization (PSO) method and two chaotic maps [37].

The characteristics of LFC for renewable energy generation in hybrid power systems are thought to depend on both the optimization method and the configuration of the

controller [38]. This paper suggests the opposition-based whale optimization algorithm (OWOA) to optimize the gains of the controller. Therefore, this work proposes an OWOA method based on FO-fuzzy-PID control for frequency and power regulation of hybrid power systems for producing renewable energy. The results of the simulation show that, unlike PID, FO-PID, fuzzy-PID, and FO-fuzzy-PID controllers, the controller under consideration can remove frequency differences well, improve supplies and provide reliable electric power going forward. In light of the aforementioned, the following elements serve as the main sources of inspiration for this study:

- Modeling the proposed HRES with an ESS system enables businesses and organizations such as hospitals, universities, and other healthcare facilities to deliver dependable power while meeting rising demand.
- The applicability of fast-response energy storage devices such as superconducting magnetic energy storage (SMES) systems and long-sustaining energy storage systems such as pumped hydro energy storage (PHES) systems for supplying quality and reliable power to meet demand can be investigated.
- The HRES with the ESS model's decision-making process is enhanced through a recently developed variation of the OWOA that is suitably tuned to manage both frequency and power variations in its major adjustable parameters.

The current study focuses on using a FO-fuzzy-PID controller with an opposition-based whale optimization technique to reduce the frequency and power oscillations that a load perturbation causes in the HRES with ES system. Based on the previous interaction, the main contributions of this research are as follows:

- The model of an HRES with ES system, which consists of two solar photovoltaic (PV) units, two biogas-generating units, two PHES units, and two SMES units, is set up in this work to demonstrate how it can be constructed.
- The FO-fuzzy-PID controller's design parameters were optimized using the OWOA metaheuristic technique.
- The proposed HRES with ES system frequency and power deviation were investigated by using PID, FO-PID, fuzzy-PID and FO-fuzzy-PID with different metaheuristic optimization techniques (such as OWOA, QOHSA, TLBOA and PSO) for tuned controller parameters.
- Disturbances were investigated bay considering the variation of connected loads, HRES sources and both of two system unites.
- The OWOA metaheuristic optimization method was adopted and used to fine-tune the different parameters that could be changed on the controllers that were being studied.
- The OWOA method was used to tune the model's parameters that could be changed. It was then compared to other optimization methods such as QOHSA, TLBOA, and PSO to see their effectiveness.

The completed work is organized as follows: Section 2 discusses the case study area, Section 3 presents how the proposed system will work, and Section 4 describes and sets up the proposed HRES with ES system. The FO-fuzzy-PID controller is introduced briefly in Section 5. Section 5 explains the problem formulation, objective function, and constraints for optimization. Section 6 presents the results and a discussion for structures in relation to variations in power output caused by load demand. The references come after Section 7, which is the conclusion of the paper.

2. Case Study Description

The developed HRES with ES system is used to power Debre Markos University, Debre Markos, Ethiopia (latitude 10.33′0″ N and longitude 37.71′0″ E). The HRES with ES system is installed to provide the required daily energy demand in the Debre Markos University. The site shown in Figure 1 has an inspiring renewable resource potential [39] that justifies its use for energizing the university, especially given its maximum interruption duration from the national gird.

3. Methodology

The proposed system is a hybrid system that is connected to the grid and can obtain power from solar PV, a biogas generator, a pumped hydro energy storage system, or a superconducting magnetic energy storage system. A first look was taken at the village's energy needs, the energy infrastructure that could be used, and the current and future renewable projects in the area. The architecture of the system is set based on the local economy and energy needs, and the best size for each power generation technology is figured out. However, the most important data, such as how much electricity was used, how much water was available for PHES, and how much biogas waste was made, came directly from the community. Solar radiation and temperature, on the other hand, are real-time meteorological data.

3.1. Connected Load Assessment

A case study is then conducted on one such remote hamlet in Debre Markos, Amhara, Ethiopia. The grid-connected hybrid renewable energy system (HRES) case study was developed to suit a community's electricity demands. Figure 2 depicts the load profile of the community on a typical worst-case-scenario day. The connected load profile is slightly increased from 1668.3000 kW to 1707.4031 kW (from 08:00–09:00 to 14:00–15:00 h), and the maximum load demand is connected during this period. Between 07:00 and 08:00, the electricity demand falls to 662.6801 kW. According to the graph below, the minimum load needs are connected to the national grid around 07:00–08:00 h in the morning.

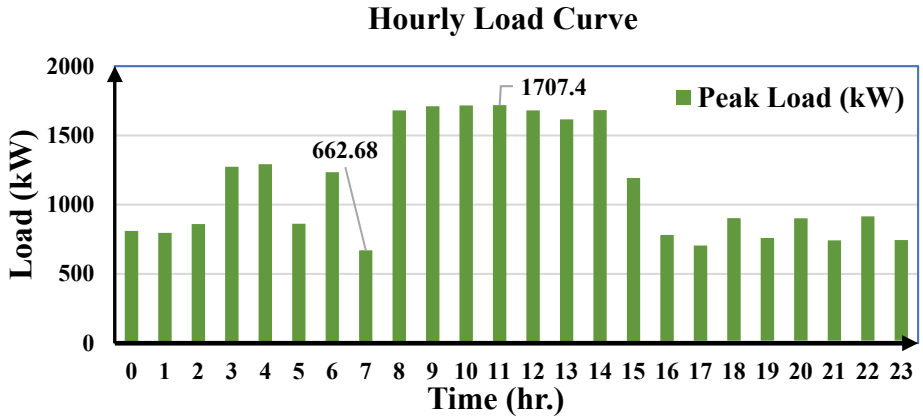

Figure 2. Community's hourly load profile on a typical worst day.

3.2. Resources Assessment

NASA's satellite meteorology and solar energy databases were used to research the temperature and amount of solar radiation in the chosen area. The monthly ambient temperature at the chosen site ranges from 16.24 to 21.46 °C. The monthly solar radiation ranges from 5.6011 to 7.8010 kWh/m^2. Figure 3 shows the monthly solar radiation and temperature values of the selected site. Figure 4 shows how the amount of daily solar radiation changes each month and how clear the area is, which suggests that the chosen site for the PV system has sufficient solar capacity. Many researchers investigated whether the selected site has sufficient solar radiation to generate solar power [39,40].

The site's potential for producing biogas was calculated using primary and secondary data received from various sources [41]. Based on the data acquired, the biogas potential of the research area is estimated to be 7.9287 × 106 m^3/year. Water resources are also available beyond the capacity of PHES energy storage technology.

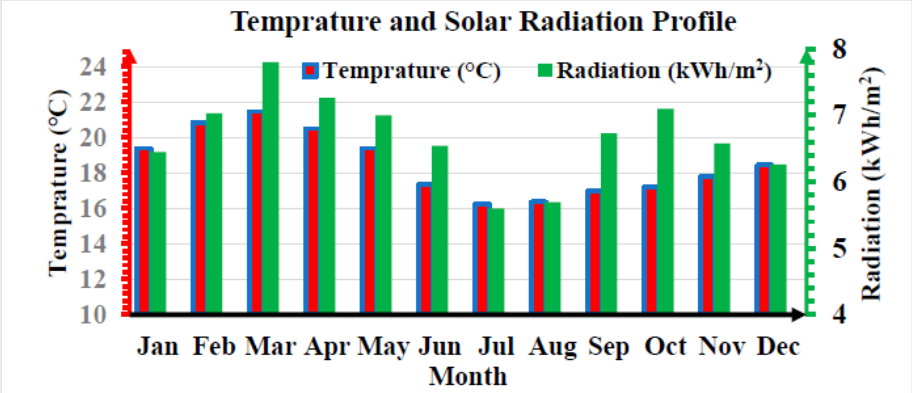

Figure 3. Average daily temperature and solar radiation on the study area.

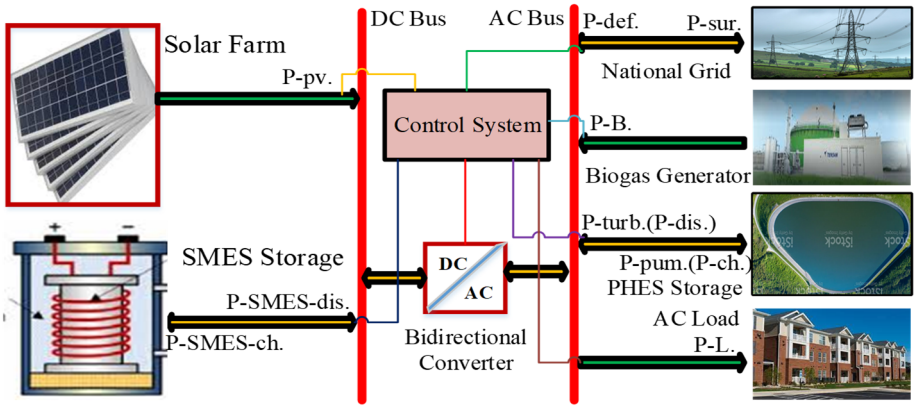

Figure 4. Schematic diagram of grid connected hybrid solar PV–biogas with hybrid SMES-PHES.

3.3. Proposed HRES with ES System Configuration and Description

The hybrid solar PV–biogas with SMES-PHES energy storage system that is connected to the national grid and, as shown in Figure 4, which consists of HRES for solar PV and biogas generators, HESS for SMES and PHES, a connection to the national grid, and AC loads connected in the system via their respective controlled power electronic converters, is being considered for quick response and long-term investigation. To obtain the most power out of solar PV systems, MPPT systems are used. When HRES's output is not sufficient to meet load demand, the primary storage system (PHES) adds power to the system. When HRES's output is too high, PHES takes power out of the system. While PHES has high reliability, it struggles with slow response times during transient conditions. SMES is therefore employed to make up for the PHES's slow dynamics. SMES has drawn energy from the system and supplied it. The hybrid system is connected to a variable load. A hybrid system's primary output is an electricity-generating energy source. If converters are part of the system model, a power converter system changes AC power to DC power and DC power to AC power. The converter converts the SMES's DC power output to the system's supplied AC power. The chopper's duty cycle and inductor current have also been limited. This plant model applies to both grid-connected and distributed power generation systems. If the power users are connected to the utility point, the hybrid system can bring in and send out power. When HRES systems have more power than they need and HESS is full, the hybrid system sends the extra power to the grid. The various technical details of the HRES component parts have been presented.

4. Mathematical Modeling of HRES with ES System

The HRES with ES system is illustrated schematically in Figure 4 using solar PV and biogas renewable energy sources with superconducting magnetic and pumped hydro energy systems. The mathematical modelling of energy sources integrated with energy

storage system is characterized using transfer functions [42,43]. Transfer functions of the first order can be used to represent the dynamics of the solar PV, biogas generator, and combinations of water pump and pump turbine analysis. The gain and time constants used to model the HRES with ES system's transfer function were adopted from different researchers [44,45].

4.1. Solar PV System Unit Modeling

The expression for the solar PV unit's output power (Figure 5) is formulated in Equation (1) [46].

$$P_{PV} = \eta_{PV} A \varphi \{1 - 0.005(T_a + 25)\} \quad (1)$$

where η_{PV} stands for photovoltaic conversion efficiency, A stands for fixed panel area (m^2), φ stands for sunshine irradiation (kw/m^2), and T_a stands for ambient temperature (°C). The η_{PV} and φ primarily influential factors of the Solar PV output power. The inverter unit is the components of a PV system that generate power efficiently.

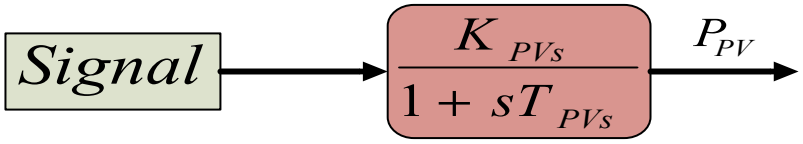

Figure 5. The Solar PV unit transfer function representation.

Additionally, the PV subsystem can be depicted as Equation (5) with a first order transfer function and lag compensation.

$$G_{PVx}(s) = \frac{K_{PV}}{1 + sT_{PV}} = \frac{\Delta P_{PV}}{\Delta \varphi} \quad (2)$$

where T_{PV} stands for the time constant carried by the PV system, and K_{PV} stands for the gain constant.

4.2. Biogas Turbine Generator Unit Modeling

The primary source of biogas is locally produced, biodegradable human and animal waste, which can be creatively recycled into electrical production using a biogas turbine generator as shown in Figure 6. The linearized model of biogas turbine generator is determined via computing (3) while accounting for the actions of the biogas inlet valve, governor, combustor, and turbine [47].

$$G_B(s) = \frac{K_{Pbiogs}}{1 + sT_{Pbiogas}} = \left(\frac{1 + sX_c}{(1 + sY_c)(1 + sb_B)}\right)\left(\frac{1 + sT_{CR}}{1 + sT_{BG}}\right)\left(\frac{K_{BG}}{1 + sT_{BT}}\right) = \frac{\Delta P_{biogas}}{\Delta f} \quad (3)$$

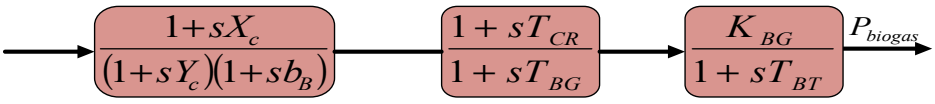

Figure 6. The biogas generator unit transfer function representation.

4.3. PHES System Unit Modeling

In pumped-storage hydroelectric systems, the use of pump and turbine components is reversible, which can have many benefits. While energy is produced by using a reversible pump turbine to run the system as a turbine during peak hours, energy can also be stored by using the pump to transfer water to the upper reservoir. Instead of generating electricity, PHES units store the energy needed during times of peak demand when supply is low. They then provide this energy when demand goes up, maintaining the HRES system's frequency stable. When hydraulic reservoirs are used, energy is produced as a result of

the hydraulic converter directly converting the potential energy into kinetic energy of the water in the channel. When the water flows, the following force is generated [48]:

$$P_h = \rho g Q \Delta h \tag{4}$$

When utilizing the transit flow method with variable water availability, the gross energy output, expressed in kWh, at a nearby hydroelectric complex can be calculated as follows:

$$P_{hA} = 9.81H \int_0^{8760} Q(t)dt \tag{5}$$

a variable flow power expressed in kW,

$$P_h = 9.81HQ(t) \tag{6}$$

The actuator, governor, hydraulic turbine, and transient droop compensator make up the pumped-storage hydro system model. Figure 7 depicts the pump-hydro system's transfer function.

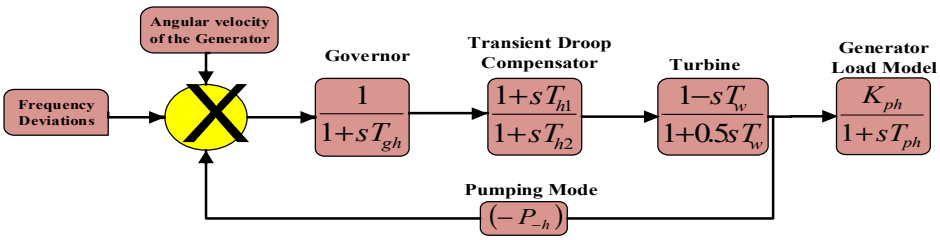

Figure 7. The pump-hydro unit transfer function representation.

During the charging mode of operation, the transfer function of PHES will be [48]:

$$G_{Ppump}(s) = \frac{K_{Ppump}}{1 + sT_{Ppump}} = \frac{\Delta P_{pump}}{(\Delta P_{PV})(1 - Kn)} \tag{7}$$

whereas during the discharging mode of operation, the transfer function of PHES will be:

$$G_{PHES}(s) = \frac{K_{Pturbine}}{1 + sT_{Pturbine}} = \left(\frac{1}{1 + sT_{gh}}\right)\left(\frac{1 + sT_{h1}}{1 + sT_{h2}}\right)\left(\frac{1 - sT_{\omega}}{1 + 0.5sT_{\omega}}\right) = \frac{\Delta P_{PVx}}{\Delta P_{Ppump}} \tag{8}$$

where T_{gh} is the actuator time constant, T_{h1} and T_{h2} are the transient droop compensator system's parameters, T_w is the water's initial flow rate through the turbine, and -P-h is the rated power for water pumping unit.

4.4. Superconducting Magnetic Energy Storage System Modeling

The magnetic field created by the current flowing through a superconductor is used to store energy in the coil. This turns into a superconductor with no resistive losses when used at cryogenic temperatures between 20 K and 77 K. More than 98% of the time is spent efficiently. The superconducting coil, transformer, and power-training unit are crucial components of the energy storage system that make it up. Other advantages of SMES units include their enormous power, high energy density, quick response time, and low maintenance costs. The superconducting coil charges when the power system is operating normally because it is powered by the AC system. The current starts to conduct with fewer electric losses at cryogenic temperatures. SMES responds more slowly than the governor control (supplemental control) and vice versa. With the aid of a converter, the

alpha communication angle is used to control the charge and discharge of the SMES. The SMES output energy can be calculated as in Equation (9) [49].

$$E_d = 2V_{do}\cos\alpha - 2I_dR_c \tag{9}$$

The SMES transfer function model is shown in Figure 8. Changes in the coil's current (ΔI_D) are interpreted as negative feedback for SMES control, which increases the coil's ability to restore its current and enable quick responses to load disturbances in the future. The equations below in (10) and (11) are displayed for changes in DC voltage and current, respectively.

$$\Delta E_D = (-K_{ID}\Delta I_D + K_F\Delta f)\left(\frac{1}{1+sT_{DC}}\right) \tag{10}$$

$$\Delta I_D = \Delta E_D\left(\frac{1}{sL}\right) \tag{11}$$

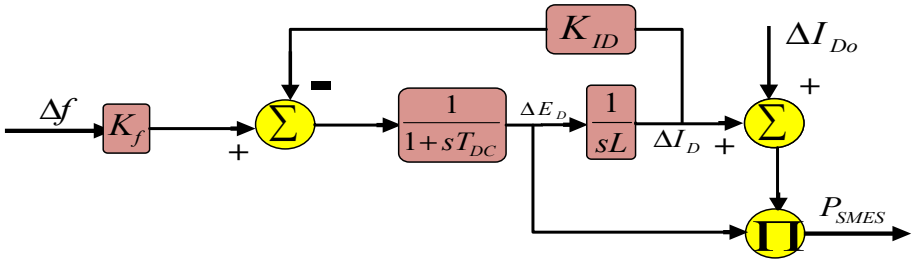

Figure 8. The SMES unit transfer function and subsystem block representation.

Finally, the SMES transfer function is expressed as in Equation (12) [21]:

$$G_{SMES}(s) = \frac{K_{SMES}}{1+sT_{SMES}} = \frac{\Delta P_{SMES}}{\Delta f} \tag{12}$$

The following shows how the SMES unit's actual power output is represented in (13):

$$\Delta P_{SMES} = \Delta E_D I_{D0} + \Delta I_D \Delta E_D \tag{13}$$

where L stands for coil inductance (H), ΔE_D for converter voltage deviation (kV), ΔI_D for coil current variation (kA), K_{ID} for ΔI_D feedback gain constant (kV/kA), and K_F for gain constant.

4.5. Proposed HRES System Dynamics Modeling

The amount of power generated and consumed determines how the system's power and frequency are changed. Each unit's transfer functions displays the amount of power generated by each generational subsystem. In Figure 9, the total output power (P_{Total}) of the HRES with ES system could be written as in (14).

$$P_{Total} = \left(P_{PV} + P_B + P_{PHES}^{Dis} + P_{SMES}^{Dis}\right) - \left(P_L + P_{PHES}^{Cha} + P_{SMES}^{Cha}\right) \tag{14}$$

Equation (15) is created when the dynamics of the HRES systems are represented in a configuration model [34].

$$G_{system}(s) = \frac{\Delta f}{\Delta P} = \frac{1}{D+sM} \tag{15}$$

In this work, the values of the inertia constant (M) and the damping constant (D) are used; M is 0.4 and D is 0.03.

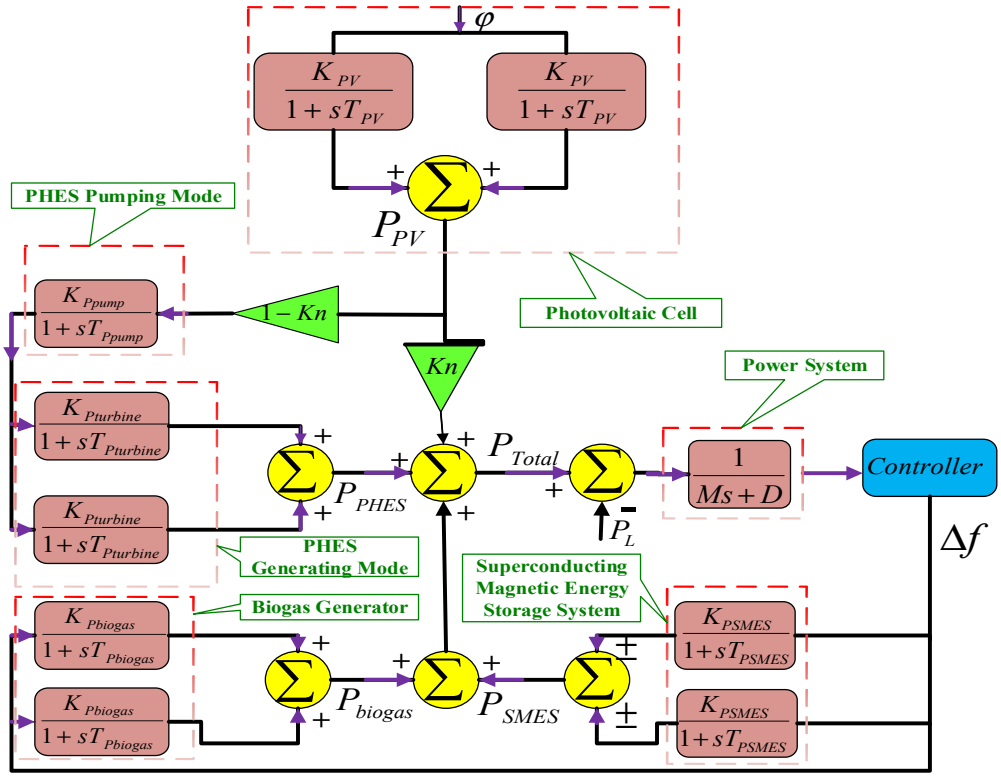

Figure 9. Schematic diagram of the HRES proposed system.

5. Proposed FO-Fuzzy-PID Controllers

For any traditional fuzzy-PID controller, the order is only taken into account as an integer value in the order of the rate of change of the error representation and the order representation of the integral at the output of the fuzzy logic controller. However, the FO-fuzzy-PID controller no longer uses integers for the rates of change of error at the input or the integral at the output. Instead, μ and λ, their equivalent tunable variables in FO, are used. A fuzzy logic controller's membership function structure has less of an impact on the effectiveness of the closed loop than Input-output variables do, which leads to the application of a scaling factor-based fuzzy logic controller. For this study, the OWOA optimization technique is used to tune the FO-fuzzy-PID controller parameters.

Das et al. introduced the FO fuzzy PID controller in [50], with [K_e, K_d] as its input scaling factors (SFs) and [K_{PI}, K_{PD}] as its output scaling factors (SFs). For applications in process control, it has been shown to produce positive results [32,51–53]. In the order of rate of change of error representation and order representation of the integral at the FLC output (i.e., μ = 1 and λ = 1 in Figure 10) for any classical fuzzy-PID controller of the FLC input level, the order is only taken into account as an integer value.

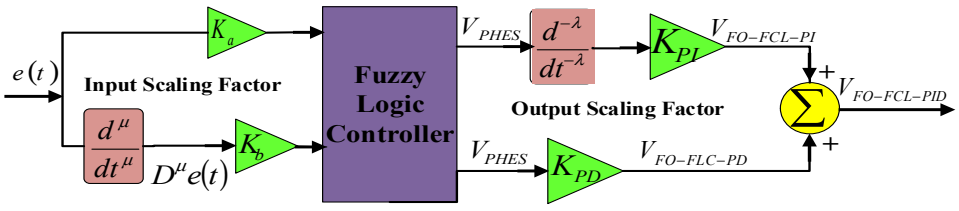

Figure 10. The proposed FO-FCL-PID controller system schematical diagram representation.

In addition, the rule base and associated membership functions for the fuzzy controller are also shown in Table 1 and Figure 11. Fuzzy linguistic variables with the letters NL, NM, NS, ZR, PS, PM, and PL denote, respectively, negative large, negative medium, negative small, zero, positive small, positive medium, and positive large. The clear output of the

fuzzy logic controller is found using the center-of-gravity method of defuzzification. The FO fuzzy controller SFs and integro-differential orders [K_e, K_d, K_{PI}, K_{PD}, μ, λ] are modified for a fixed rule base and membership function type using the opposition-based whale optimization algorithm. However, the FO-Fuzzy-PID controller's FLC no longer uses integers to determine the order of the "rates of change of error" at the input and the integral at the output. Instead, they are replaced by the corresponding tunable variables, namely μ and λ, of their FO counterparts.

Table 1. Rule base for error, FLC output and fractional rate of error.

$\frac{d^\mu U}{dt^\mu}$ \ U	NL	NM	NS	Z	PS	PM	PL
NL	PL	PM	PS	PS	Z	PS	Z
NM	PS	PS	PM	PS	NL	NM	NM
NS	PL	PM	PM	PM	Z	NS	NS
Z	NL	NM	NS	Z	NS	PM	PL
PS	PM	PS	PS	Z	PS	PS	PS
PM	PS	PS	PM	PM	Z	NS	NL
PL	Z	PS	PM	Z	NS	NM	NL

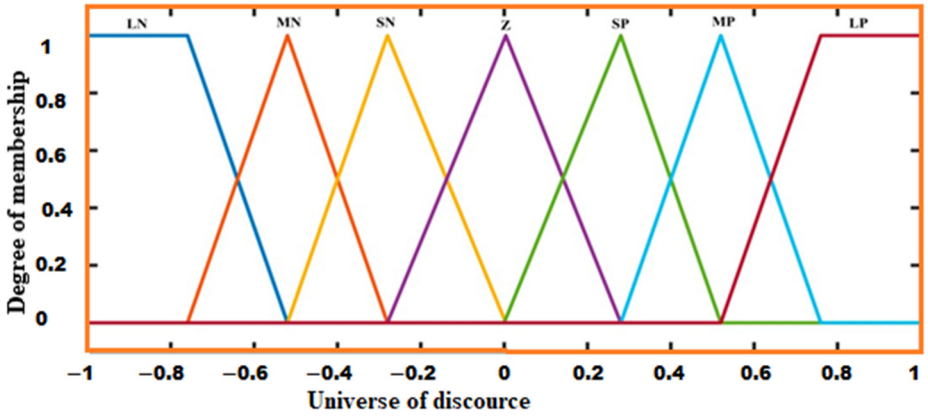

Figure 11. Schematic representation of membership function for error, FLC output, and fractional derivative of error.

One of several continuous and discrete-time rational approximation methods for fractional order elements can be seen as the heart of the proposed fuzzy logic-based fractional order controller [54–56]. The Oustaloup 5th order rational approximation is used in the current paper to continuously justify each guess value of the fractional order differ-integrals [μ, λ] within the optimization process. In essence, infinite-dimensional linear filters are what the FO differ-integrators are. However, for practical implementation, band-limited realizations of fractional order controllers are required. In this study, each fractional order element was interpreted using the Oustaloup recursive filter, which is illustrated in Equations (16) and (17). If we assume that the frequency range or expected fitting range of the controller is [ω_b,ω_h], then the higher order filter that most closely resembles the FO element S^α can be expressed as follows [57]:

$$G_f(s) = S^\alpha \approx K \prod_{K=-N}^{N} \left(\left(s + \omega_K^! \right) \Big/ \left(s + \omega_K \right) \right) \tag{16}$$

The filter's poles, zeros, and gain can be assessed as follows:

$$\begin{aligned} \omega_K &= \omega_b \left({\omega_h}/{\omega_b} \right)^{{(K+N+(1+\alpha)/2)}/{(2N+1)}} \\ \omega_K^{!} &= \omega_b \left({\omega_h}/{\omega_b} \right)^{{(K+N+(1-\alpha)/2)}/{(2N+1)}}, K = \omega_h^{\alpha} \end{aligned} \tag{17}$$

In Equations (16) and (17), α is the order of the differencing integration which ranges from $0 < \alpha < 1$ and $|2N + 1|$ is the order of the realized analogue filter. This work considers a 5th-order Oustaloup approximation for all FO elements in the frequency range $\omega \in \left[10^{-2}, 10^{2}\right]$ rad/s.

In the context of this work, it is assumed that an FLC's rule base and MFs are not both optimized for FO-fuzzy-PID controllers and conventional fuzzy-PID [58–60]. To achieve the best enactment, the I/O SFs (K_a, K_b, K_{PI}, and K_{PD}) are optimized in the fractional rate of error (i.e., μ) and FO integration (i.e., λ) of FLC output (FO-Fuzzy-PID). Table 1 provides the FLC's rule base, and Figure 11 presents fixed-shaped MFs.

5.1. Problem Formulations

The primary goal of the current research is to guarantee that the response profiles of the examined HRES and ES system models have a minimum frequency deviation and power deviation.

5.2. Objective Function

To set the controller parameters, the objective function is chosen. A decrease in overshoot, undershoot, and settling time is the system's desired dynamic response. The LFC control techniques that have been used state that the feedback system must meet the stability requirement and that the integral frequency error must be less than the specified low threshold value or close to zero. The main performance criteria for the present work is the integral of absolute error (IAE) considered. To design a controller, the objective function is primarily specified based on this parameter. Previous research has demonstrated that, of the three, the ISE objective function offers the best system performance. In this study, ISE was chosen as the objective function for the single area power system. It is written as [1,61,62]:

$$Min\{ISE(\Delta f)\} = Min\left\{ ISE(\Delta f) = \int_0^{\infty} |\Delta f|^2 dt \right\} \tag{18}$$

where Δf represents a deviation in frequency.

5.3. Constraints

The optimization problem in the employed HRES with ES system model has constraints for optimizing a number of tunable variables. When minimizing the objective function for this study, the constraints of the objective function are given in Equation (19).

$$\left.\begin{array}{c} K_P^{\min} \le K_P \le K_P^{\max} \\ K_I^{\min} \le K_I \le K_I^{\max} \\ K_D^{\min} \le K_D \le K_D^{\max} \\ K_{PI}^{\min} \le K_{PI} \le K_{PI}^{\max} \\ K_{PD}^{\min} \le K_{PD} \le K_{PD}^{\max} \\ \mu^{\min} \le \mu \le \mu^{\max} \\ \lambda^{\min} \le \lambda \le \lambda^{\max} \end{array}\right\} \tag{19}$$

The minimum and maximum values of the parameters of the PID/FO-PID/fuzzy-PID/FO-fuzzy-PID controller in HRES with ES systems are denoted by the min and max, respectively. The optimized K_P, K_I, K_D, K_{PI}, and K_{PD} parameters' boundaries are chosen

from a range of 0 to 100, while the μ and λ are chosen from a range of 0 to 1. The algorithm used for this particular work is the opposition-based whale optimization algorithm (OWOA), which is introduced by Alamri et al. [63], who provided its pseudo-code. When the optimization process was complete, the program could output an ISE value. To evaluate the performance of different controllers, additional performance metrics are examined and compared in order to identify the most efficient controller [64]. Finally, quasi-oppositional harmony search algorithm (QOHSA) [9,65–67], teaching learning based optimization algorithm (TLBOA) [68] and particle swarm optimization (PSO) algorithm [13,33,36,69] are used for comparison with the OWOA results.

6. Result and Discussion

The investigation of the HRES with ES system model considers the outcomes of time-domain executions under various, distinct perturbation conditions. Under normal operating circumstances, it is assumed that the total load demand will be 1 p.u. Unexpected drops or increases in P_L and PV are correctly used at specified time instants for the system being used to investigate the effects of a sudden change in demanded load or solar PV irradiation (φ) on the HRES with ES system model's closed-loop response. Figure 1 with a controlling action is referred to as FO-fuzzy-PID for simulation purposes in this work. The effectiveness of the opposition-based whale optimization algorithm in maximizing various controller (i.e., PID, FO-PID and fuzzy-PID) parameters is examined in this paper using different situations. The following scenarios are the input perturbation conditions:

- Scenario 1: Disturbances caused by load fluctuation.
- Scenario 2: Disturbance is limited to HRES with ES system.
- Scenario 3: Disturbance from both the load and HRES with ES system.
- Scenario 4: Sensitivity analysis of the integrated power system.

Scenario 1: Disturbances caused by load fluctuation

In order to assess the effectiveness of the optimized values produced by the suggested opposition-based whale optimization algorithm, the studied power system model is operated under load variation ranging from 0.15 p.u. to 0.56 p.u., as shown in Figure 12.

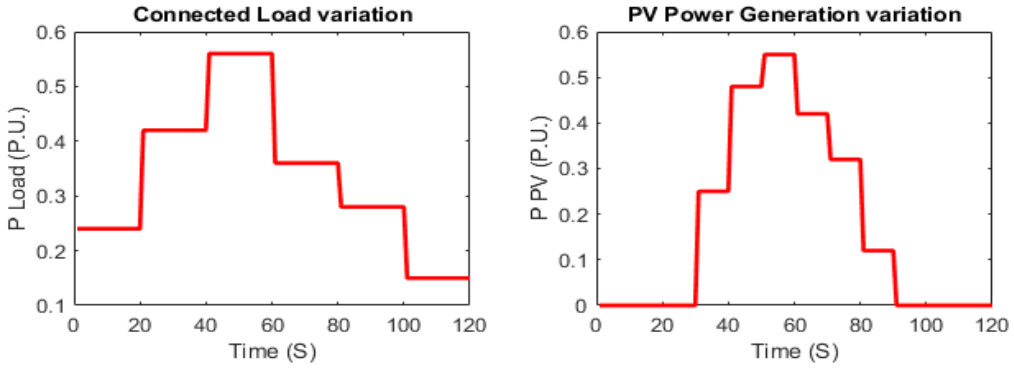

Figure 12. Graphical representation of connected load and PV generation step variation.

Figures 13 and 14 show, separately, the patterns of ΔF (Hz) and ΔP (p.u.) with load demand for PID, FO-PID, fuzzy-PID, and FO-fuzzy-PID of the investigated HRES with ES system model by utilizing different metaheuristic optimization techniques such as OWOA, QOHSA, TLBOA and PSO. Figures 13 and 14 show that the proposed FO-fuzzy-PID model configuration outperforms the three other model configurations (i.e., PID, FO-PID and fuzzy-PID) in terms of performance criteria and has less maximum overshoot. The output power with the best system implementation is achieved with the suggested FO-fuzzy-PID controller using OWOA. As shown in Figures 13 and 14, the OWOA technique is better than other optimization methods in solving the optimization problem.

In all optimization techniques, the proposed FO-fuzzy-PID controller achieves minimum frequency and power deviations. Figure 15 shows how the frequency and power

deviation parameters of the FO-fuzzy-PID controller are evaluated using OWOA, QOHSA, TLBOA, and PSO. As shown in Figure 16, OWOA achieves the best results compared to the other methods.

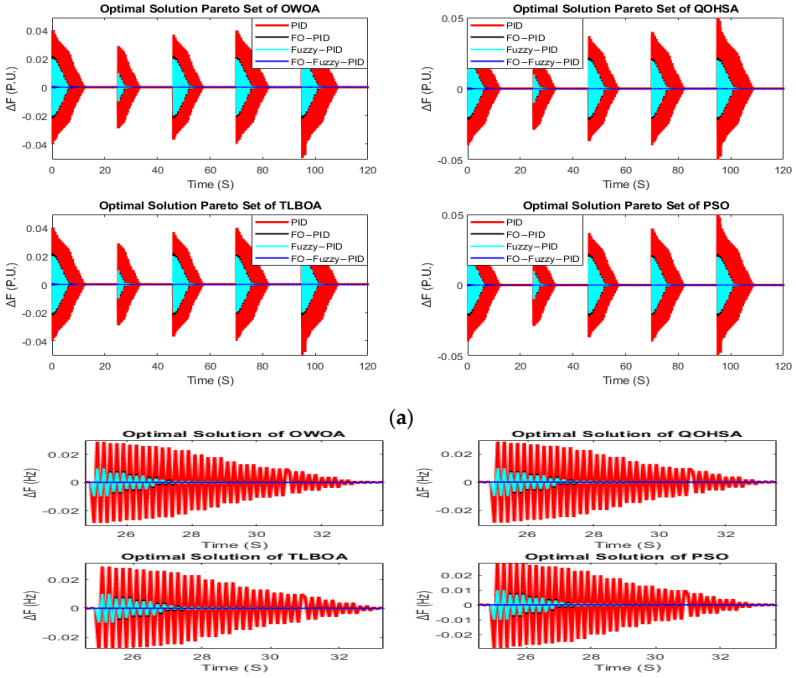

Figure 13. Frequency deviation in the nonlinear response of HRES (**a**) with stepwise load changes (**b**) constant solar power production using OWOA, QOHSA, TLBOA and PSO tuned controllers.

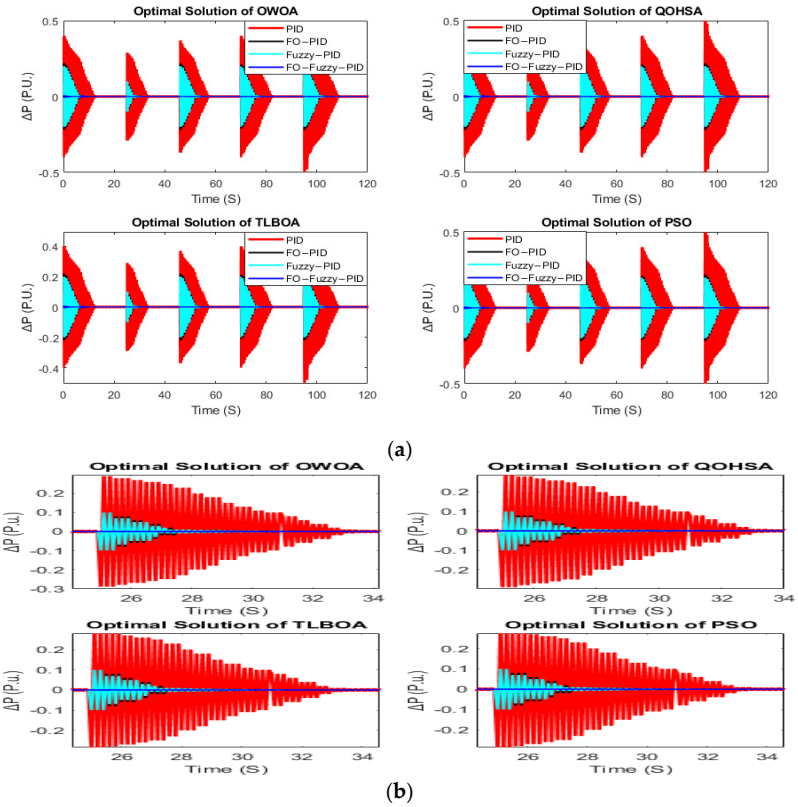

Figure 14. Power deviation in the nonlinear response of HRES with (**a**) stepwise load changes (**b**) constant solar power production using OWOA, QOHSA, TLBOA and PSO tuned controllers.

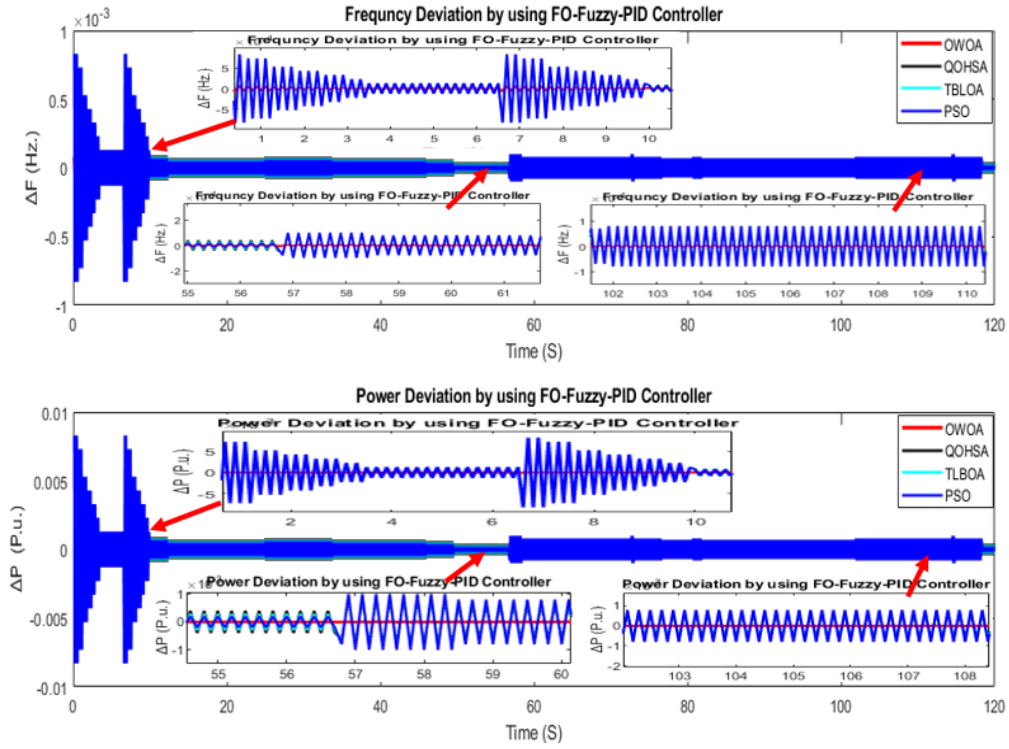

Figure 15. ΔF and ΔP on FO-fuzzy-PID result comparison using OWOA, QOHSA, TLBOA and PSO.

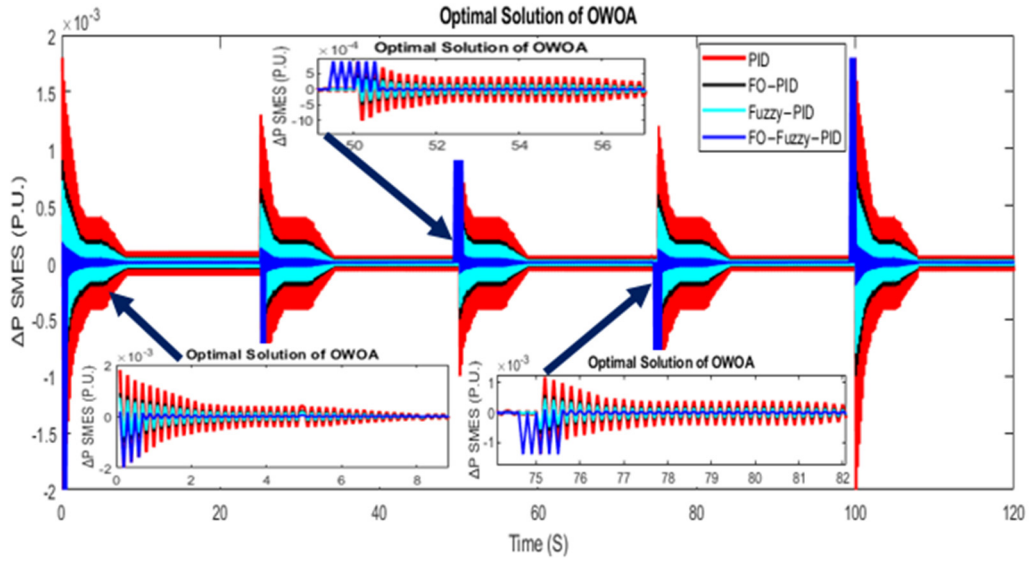

Figure 16. Power deviation in the nonlinear response of SMES system under constant solar output power and variable load conditions using OWOA-tuned controllers.

According to Figure 12, the OWOA results are far better than those of the other metaheuristic optimization techniques. As a result, OWOA will be used for additional research throughout the course of this work. As shown in Figures 16 and 17, power deviation is represented in the nonlinear response of SMES, biogas and PHES system utilizing OWOA. In all aspects, the FO-fuzzy-PID controller achieves the optimal solution for this study.

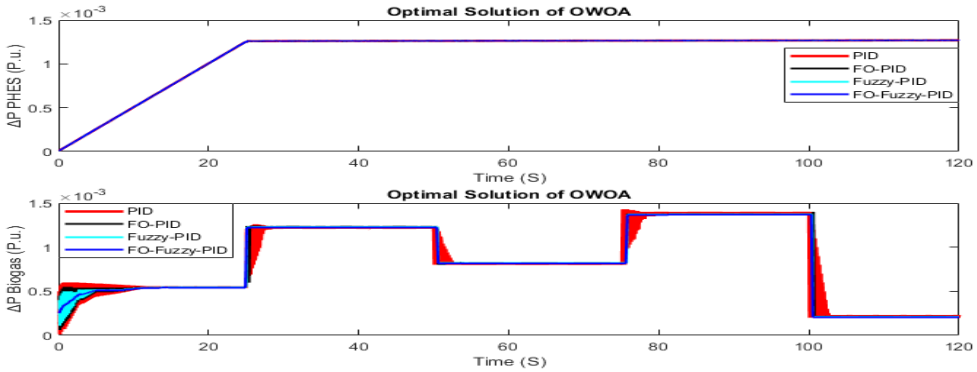

Figure 17. Power deviation in the nonlinear response of biogas and PHES system under constant solar output power and variable conditions using OWOA-tuned controllers.

It is important to keep in mind that there are specific HRES with ES system components where it can be determined that there is a significant gap between the output of the PID, FO-PID, fuzzy-PID and FO-fuzzy-PID controllers, with the FO-fuzzy-PID controller case showing the least amount of power differences. As a result, the analyzed HRES with ES system model's FO-fuzzy-PID is set up to be stronger than the other three model configurations. The numerical approximations of transient parameters for the well-known perturbation are listed in Table 2 alongside the other controllers.

Table 2. Transient response parameters of the HRES with controllers for scenario 1.

Disturbance	Controller	Transient Response Parameters of ΔF			Performance Index
		Undershoot (p.u)	Overshoot (p.u)	Settling Time (Sec)	ISE
Load Perturbation	PID	82.32×10^{-3}	74.71×10^{-3}	10.53	19.3×10^{-5}
	FO-PID	9.46×10^{-3}	5.14×10^{-3}	6.23	10.7×10^{-5}
	Fuzzy-PID	8.52×10^{-3}	4.62×10^{-3}	5.65	8.4×10^{-5}
	FO-fuzzy-PID	6.41×10^{-3}	2.98×10^{-3}	3.12	3.2×10^{-5}

Furthermore, Table 3 shows the controller configurations that work well in this scenario for integrating different HRES and ES system configurations.

Table 3. Optimized values of the controller under consideration for various HRES with ES system configurations for scenario 1.

Parameters	Types of Controllers			
	PID	FO-PID	Fuzzy-PID	FO-Fuzzy-PID
KP	98.72	90.47	89.52	-
KI	12.35	91.72	93.83	-
KD	29.61	60.26	73.29	-
KPI	-	-		95.32
KPD	-	-		86.85
KA	-	-		0.88
KB	-	-		0.71
λ	-	0.81		0.97
μ	-	0.92		0.93

Scenario 2: Disturbance is limited to HRES with ES system

To evaluate the effectiveness of the optimized gains produced by the opposition-based whale optimization algorithm, the studied power system model was subjected to a perturbation of solar PV generation from 0.12 to 0.55 p.u. without load perturbation. Figures 18 and 19 illustrate the characteristics of ΔF (Hz) and ΔP (p.u.) considering the perturbation of solar PV generation (shown in Figure 12) for the various configurations of HRES with ES system model (such as PID, FO-PID, fuzzy-PID, and FO-F-PID).

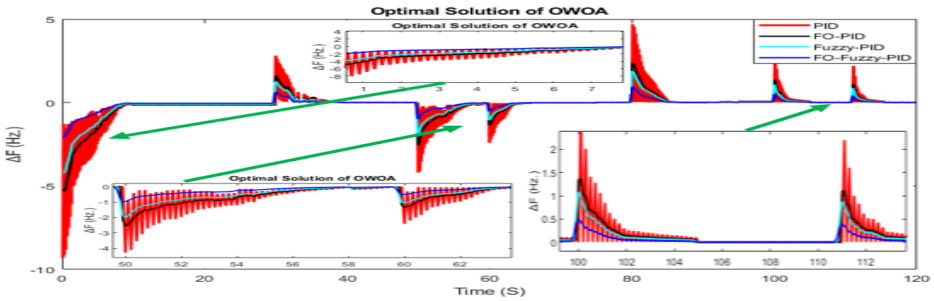

Figure 18. Frequency deviation in the nonlinear response of HRES with stepwise solar power production variations and constant connected load using OWOA-tuned controllers.

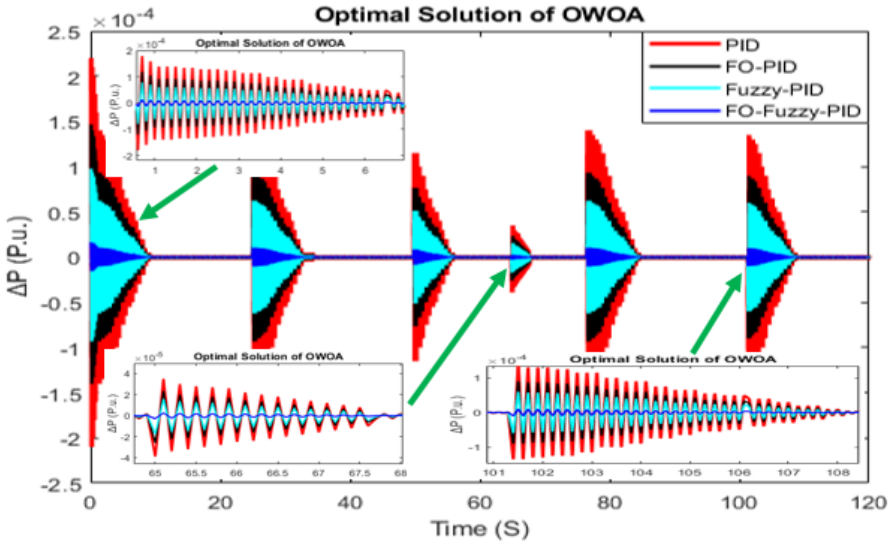

Figure 19. Power deviation in the nonlinear response of HRES with stepwise solar power production variations and constant connected load using OWOA-tuned controllers.

The recommended FO-fuzzy-PID controller achieves the best HRES with ES system performance, as shown in Figures 18 and 19; in terms of steady-state error, overall overshoot (i.e., less maximum overshoot), and settling time, the proposed FO-fuzzy-PID configuration outperforms the PID, FO-PID and fuzzy-PID configurations. The power output of SMES, biogas and the PHES system is shown in Figures 20 and 21, where it is possible to observe the significant differences in performance between the PID, FO–PID, fuzzy-PID and FO–fuzzy–PID controllers.

There are fewer power variations with the FO-fuzzy-PID controller. As a result, it is possible to conclude that FO-fuzzy-PID controllers with OWOA outperform PID, FO-PID and fuzzy-PID controllers with OWOA-tuned controllers. In Table 4, the numerical estimates of the transient controller parameters demonstrate how the FO-fuzzy-PID controller outperforms the fuzzy-PID, FO-PID and PID controllers in terms of performance.

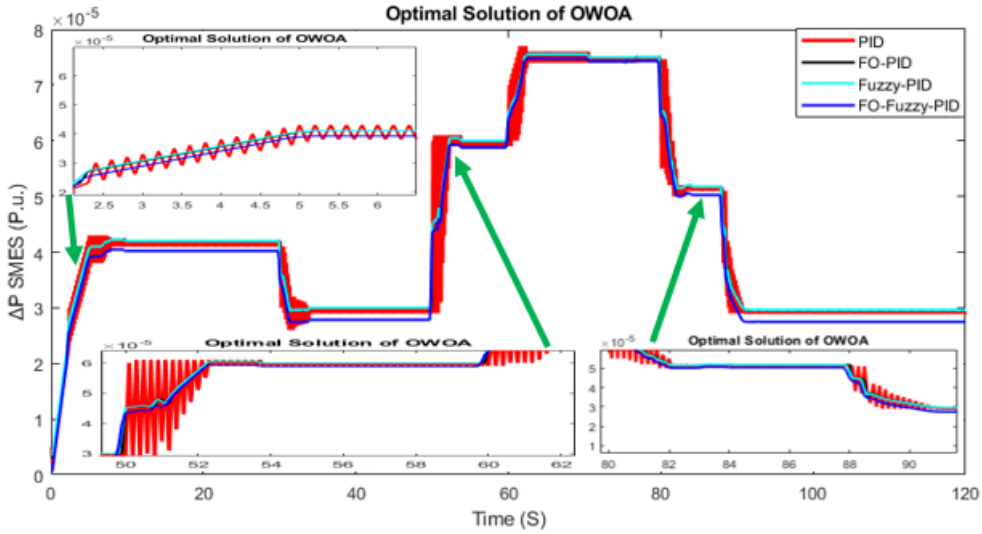

Figure 20. For Scenario 2, Power deviation in the nonlinear response of SMES system under constant load and variable solar output power conditions using OWOA-tuned controllers.

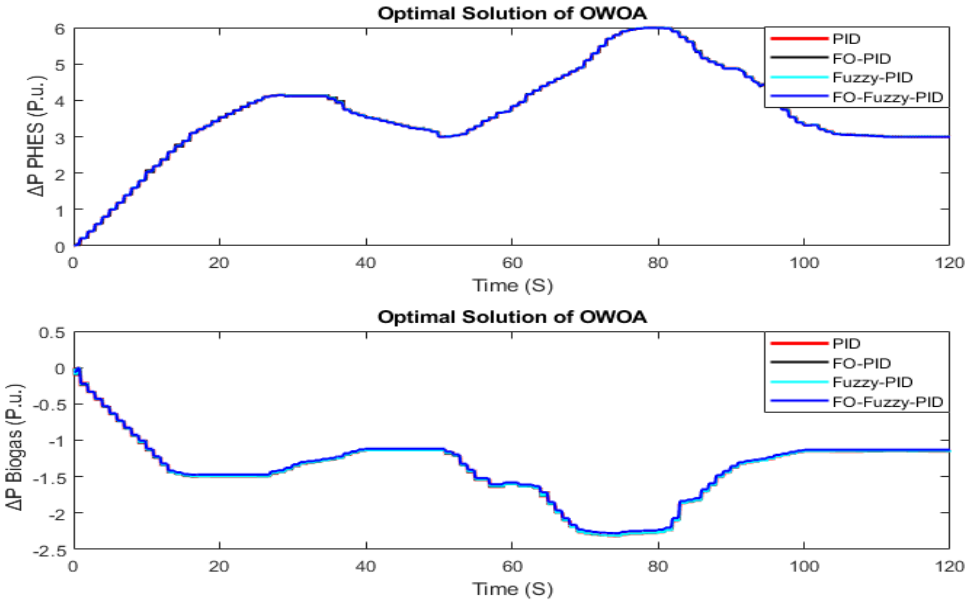

Figure 21. For Scenario 2, Power deviation in the nonlinear response of biogas and PHES system und constant load and variable solar output power conditions using OWOA-tuned controllers.

Table 4. Transient response parameters of the HRES with controllers for scenario 2.

Disturbance	Controller	Transient Response Parameters of ΔF			Performance Index
		Undershoot (p.u)	Overshoot (p.u)	Settling Time (Sec)	ISE
Load Perturbation	PID	15.85×10^{-3}	7.35×10^{-3}	9.28	3.36×10^{-5}
	FO-PID	8.64×10^{-3}	3.07×10^{-3}	6.04	2.03×10^{-5}
	Fuzzy-PID	6.08×10^{-3}	2.16×10^{-3}	5.11	1.05×10^{-5}
	FO-fuzzy-PID	3.73×10^{-3}	0.95×10^{-3}	4.03	0.32×10^{-5}

Table 5 shows the best values of the controllers for the different HRES with ES system configurations, as well as numerical estimates of the transient controller parameters for this scenario.

Table 5. Optimized values of the controller under consideration for various HRES with ES system configurations for Scenario 2.

Parameters	Controllers			
	PID	**FO-PID**	**Fuzzy-PID**	**FO-Fuzzy-PID**
KP	97.89	97.87		-
KI	99.75	92.53		-
KD	37.55	35.94		-
KPI	-	-		83.28
KPD	-	-		89.75
KA	-	-		0.95
KB	-	-		0.42
μ	-	0.98		0.89
λ	-	0.39		0.72

Scenario 3: Disturbance from both the load and HRES with ES system

In order to evaluate the effectiveness of the optimized gains produced by the considered algorithm (i.e., OWOA), the undertaken HRES with ES system model was subjected to load perturbation and solar PV generation variation from 0.1 to 0.5 p.u. and 0.15 to 0.3 p.u., respectively, as shown in Figure 12. Figures 22 and 23 show the shapes for ΔF (Hz) and ΔP (p.u.) due to perturbation from the load and solar PV generation (as shown in Figure 12) for the different configurations of the controllers undertaken HRES with ES system, namely PID, FO-PID, fuzzy-PID and FO-fuzzy-PID. The suggested FO-fuzzy-PID controller enhances system performance, as shown in Figures 22 and 23. In terms of steady-state error, maximum overshoot (i.e., smaller maximum overshoot), and settling time, the suggested FO-fuzzy-PID configuration outperforms the PID, FO-PID and fuzzy-PID configurations.

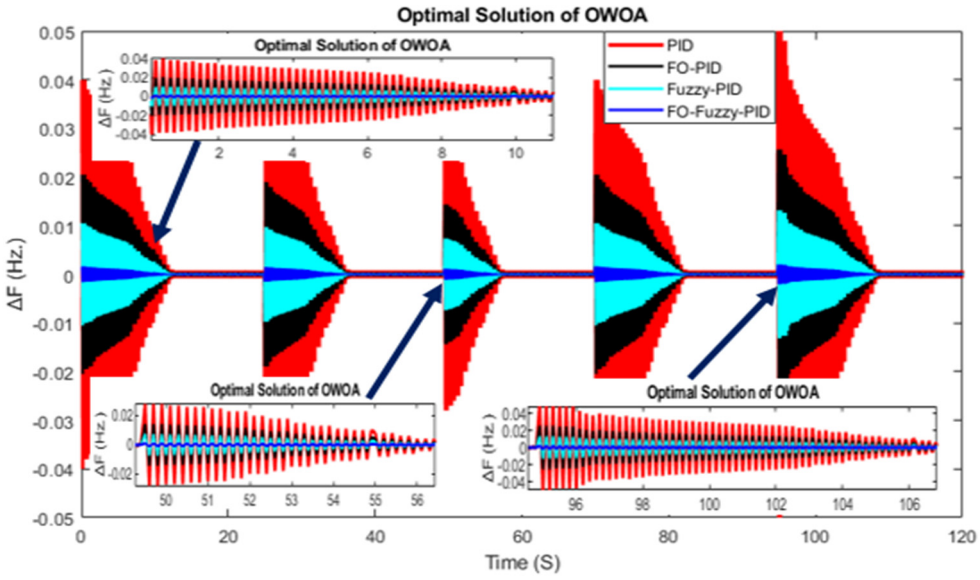

Figure 22. For Scenario 3, Frequency deviation in the nonlinear response of HRES with stepwise variations of solar power production and connected load using OWOA-tuned controllers.

Figures 24 and 25 depict the power output of the various HRES sources, demonstrating how the PID, FO-PID, and FO-fuzzy-PID controllers behave very differently, despite the FO-fuzzy-PID controller having less power fluctuation. In comparison with the OWOA-tuned PID and FO-PID controllers, it is safe to say that the OWOA-tuned FO-fuzzy-PID controller provides the best system responses. The transient parameters for scenario 3 is

contrasted with the parameters for other controllers in Table 6. Table 7 shows the best value for the controller under consideration for the different ways HRES systems can be set up.

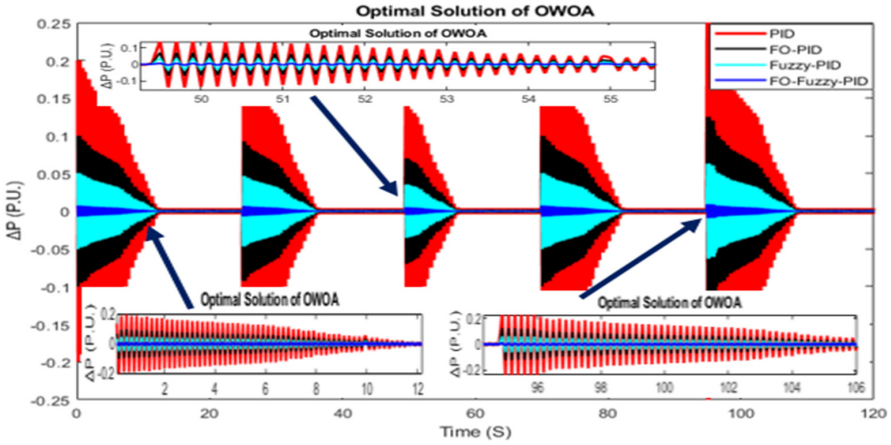

Figure 23. For Scenario 3, Power deviation in the nonlinear response of HRES with stepwise variations of solar power production and connected load using OWOA-tuned controllers.

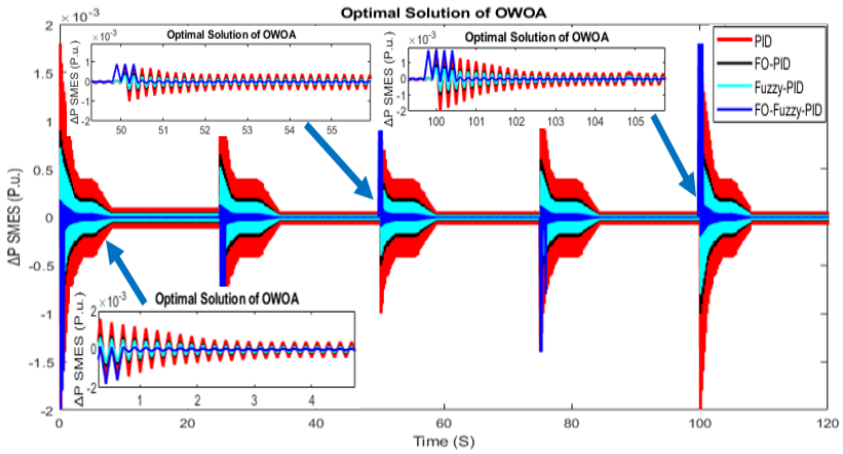

Figure 24. For Scenario 3, Power deviation in the nonlinear response of SMES system under constant load and variable solar output power conditions using OWOA-tuned controllers.

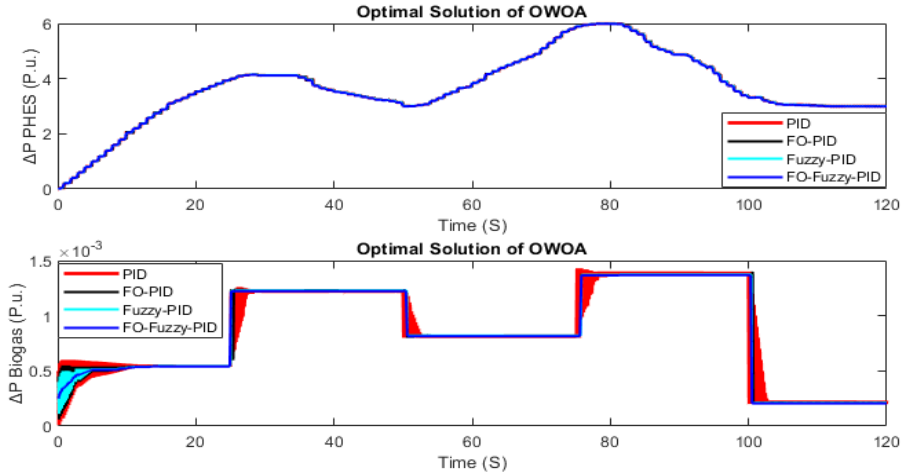

Figure 25. For Scenario 3, Power deviation in the nonlinear response of biogas and PHES system under constant load and variable solar output power conditions using OWOA-tuned controllers.

Table 6. Transient response parameters of the HRES with controllers for scenario 3.

Disturbance	Controller	Transient Response Parameters of ΔF			Performance Index
		Undershoot (p.u)	Overshoot (p.u)	Settling Time (Sec)	ISE
Load Perturbation	PID	73.82×10^{-3}	71.55×10^{-3}	13.87	13.52×10^{-5}
	FO-PID	9.85×10^{-3}	10.91×10^{-3}	7.83	7.05×10^{-5}
	Fuzzy-PID	5.74×10^{-3}	6.02×10^{-3}	4.08	2.36×10^{-5}
	FO-fuzzy-PID	2.98×10^{-3}	2.04×10^{-3}	2.01	1.08×10^{-5}

Table 7. Optimized values of the controller under consideration for various HRES with ES system configurations for Scenario 3.

Parameters	Controllers			
	PID	FO-PID	Fuzzy-PID	FO-Fuzzy-PID
KP	97.88	98.97	97.01	-
KI	98.92	93.58	94.31	-
KD	91.05	37.64	41.25	-
KPI	-	-		84.32
KPD	-	-		97.16
KA	-	-		0.49
KB	-	-		0.33
μ	-	0.88		0.82
λ	-	0.94		0.93

Scenario 4: Sensitivity analysis of the integrated power system

In this scenario, the proposed controller's sensitivity is analyzed against variations in the power system's block parameters of HRES with ES system from their nominal values, which is tabulated in Table 8.

Table 8. Nominal values of HRES components.

HRES Units	Gain	Time Constant	Rating
PV	KPV = 1.000	TPV = 1.935	13,000 kW
Biogas	Kbiogas = 0.0042	Tbiogas = 3.001	875 kW
SMES	KSMES = −0.035	TSMES = 0.052	120 kWh
Pump	Kpump = 0.02	Tpump = 3.25	
PHES	KPHES = 0.01	TPHES = 4.1	600 kW

The suggested frequency and power deviation controller works by comparing the percentage of difference caused by changes to the parameters of the power system block (i.e., vectors M and D) with the value of the objective function.

The ΔF and ΔP profiles that are produced in relation to one of the agreed-upon constants are simultaneously subject to change, while the other constant is kept at its nominal value in Figure 26, and the performance measurements are noted. As a general rule in this section, when the values of the parameters of the power system block (i.e., vectors M and D) are changed significantly, there cannot be a change in significant values on frequency and power deviations underutilization of FO-fuzzy-PID controller tuned by OWOA.

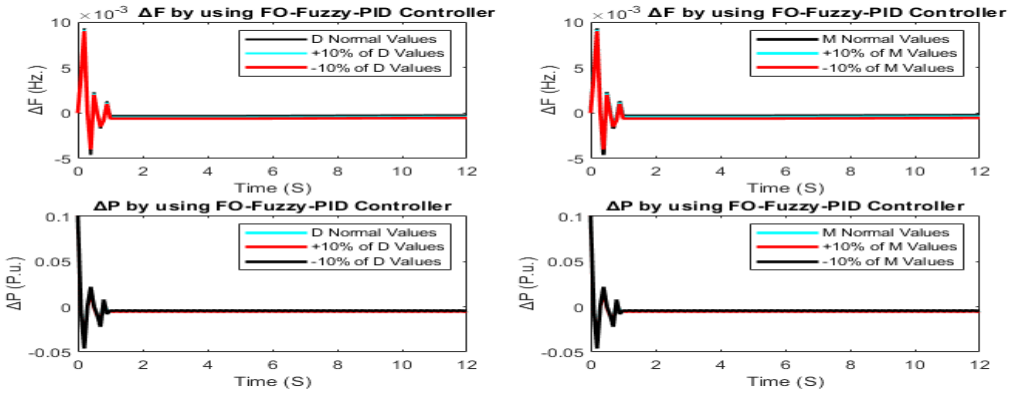

Figure 26. Sensitivity investigation of the HPS with the FO-fuzzy-PID controller for ±10% variations in D&M.

As a result, even with changing parameters, the suggested controller, optimized with the OWOA, convincingly demonstrates its robustness for controlling frequency and power in the HRES with ES system model. The results in Table 8 show that the FO-fuzzy-PID controller is robust against significant parameter fluctuations.

As shown in Table 9, the values of ISE are minimum, which means the proposed research findings have been achieved since the goal of this research was to minimize the numerical values of the objective function (ISE) under consideration of constraints.

Table 9. Analysis of sensitivity to variations in system parameters.

Parameters	Changing Rate	ISE
Normal	0	0.00201×10^{-3}
D	+10%	0.00262×10^{-3}
	−10%	0.00254×10^{-3}
M	+10%	0.00265×10^{-3}
	−10%	0.00247×10^{-3}

7. Conclusions

This study proposes a HRES (i.e., solar PV and biogas generator) with an ES (superconducting magnetic and pumped hydro energy storage) system modelling and control system by using a recent controller as part of a centralized control scheme to minimize frequency and power oscillation in a hybrid power system. Classical controllers may not be as effective in addressing load frequency control issues, especially when nonlinearities and random load perturbations are present, along with electricity generated by solar PV production systems. A FO-fuzzy-PID controller is suggested for the current study for hybrid energy supply frequency control such as solar, biogas generators, and energy storage systems, such as superconducting magnetic energy storage or pumped hydro energy storage, in order to enhance the system's performance. In order to simplify the control system, save on maintenance costs, and reduce the number of control variables, a centralized control scheme has been implemented. The key conclusions of the study are listed as follows:

- When the load and solar irradiation disrupt the system, the PID, FO-PID and fuzzy-PID controllers' configuration performs remarkably well to suppress the frequency and power oscillations of the system.
- PID/FO-PID/fuzzy-PID/FO-fuzzy-PID controllers tuned with different metaheuristic optimization techniques (OWOA, QOHS, TLBOA, and PSO algorithms) have been proposed and implemented on HRES with ESS; as a result, OWOA is given priority and used throughout this work.

- Compared to the other system configurations that were taken into consideration, the FO-fuzzy-PID controller combination performs incredibly well and successfully reduces the oscillation of the system.
- The FO-fuzzy-PID control technique outperforms the competition and is stable and robust in the face of random load perturbations, altered system parameters, and system nonlinearities.

When QOHSA, TBLOA, and PSO have been used to tune, respectively, the results of the frequency deviation obtained using FO-fuzzy-PID controllers with OWOA tuning are, respectively, 1.05%, 2.01%, and 2.73% lower. The proposed HRES with ES system model uses the OWOA technique, which has a highly effective computational performance, to enhance the FO-fuzzy-PID controller parameter for control of frequency and power.

Author Contributions: Conceptualization, T.F.A., A.F.-L., B.K. and E.T.; methodology, T.F.A., A.F.-L., B.K. and E.T.; software, T.F.A., A.F.-L., B.K. and E.T.; validation, T.F.A., A.F.-L., B.K. and E.T.; formal analysis, T.F.A., A.F.-L., A.A., I.A., B.K., M.E., O.P.M., R.M.Á. and E.T.; investigation, T.F.A., A.F.-L., B.K. and E.T.; resources, T.F.A., A.F.-L., A.A., I.A., B.K., M.E., O.P.M., R.M.Á. and E.T.; data curation, T.F.A., A.F.-L., A.A., I.A., B.K., M.E., O.P.M., R.M.Á. and E.T.; writing—original draft preparation, T.F.A., A.F.-L., B.K. and E.T.; writing—review and editing, T.F.A., A.F.-L., B.K. and E.T.; visualization, T.F.A., A.F.-L., B.K. and E.T.; supervision, A.F.-L., B.K. and E.T.; project administration, FA, A.F.-L., A.A., I.A., B.K., M.E., O.P.M., R.M.Á. and E.T. All authors have read and agreed to the published version of the manuscript.

Funding: This research received no external funding.

Institutional Review Board Statement: Not applicable.

Informed Consent Statement: Not applicable.

Data Availability Statement: Data will be available on request.

Acknowledgments: The authors kindly thank the Editor and reviewers who spent their valuable time improving the present paper. Takele Ferede Agajie kindly thanks the financial support of the MIRET Scholarship program through project No: 614658-PANAF-1-2019-1-KE-PANAF-MOBAF.

Conflicts of Interest: The authors declare no conflict of interest.

References

1. Mukherjee, V. A novel quasi-oppositional harmony search algorithm and fuzzy logic controller for frequency stabilization of an isolated hybrid power system. *Int. J. Electr. Power Energy Syst.* **2015**, *66*, 247–261.
2. Tarkeshwar, M.; Mukherjee, V. Quasi-oppositional harmony search algorithm and fuzzy logic controller for load frequency stabilisation of an isolated hybrid power system. *IET Gener. Transm. Distrib.* **2015**, *9*, 427–444. [CrossRef]
3. Ali, A.; Shakoor, R.; Raheem, A.; Muqeet, H.A.U.; Awais, Q.; Khan, A.A.; Jamil, M. Latest Energy Storage Trends in Multi-Energy Standalone Electric Vehicle Charging Stations: A Comprehensive Study. *Energies* **2022**, *15*, 4727. [CrossRef]
4. Alayi, R.; Zishan, F.; Seyednouri, S.R.; Kumar, R.; Ahmadi, M.H.; Sharifpur, M. Optimal Load Frequency Control of Island Microgrids via a PID Controller in the Presence of Wind Turbine and PV. *Sustainability* **2021**, *13*, 10728. [CrossRef]
5. Naware, D.; Thogaru, R.B.; Mitra, A. Integration of Renewable Sources and Energy Storage Devices. In *Planning of Hybrid Renewable Energy Systems, Electric Vehicles and Microgrid*; Springer: Berlin/Heidelberg, Germany, 2022; pp. 759–783. [CrossRef]
6. Boudia, A.; Messalti, S.; Harrag, A.; Boukhnifer, M. New hybrid photovoltaic system connected to superconducting magnetic energy storage controlled by PID-fuzzy controller. *Energy Convers. Manag.* **2021**, *244*, 114435. [CrossRef]
7. Makhdoomi, S.; Askarzadeh, A. Impact of solar tracker and energy storage system on sizing of hybrid energy systems: A comparison between diesel/PV/PHS and diesel/PV/FC. *Energy* **2021**, *231*, 120920. [CrossRef]
8. Ranjan, M.; Shankar, R. A literature survey on load frequency control considering renewable energy integration in power system: Recent trends and future prospects. *J. Energy Storag.* **2021**, *45*, 103717. [CrossRef]
9. Shankar, G.; Mukherjee, V. Load frequency control of an autonomous hybrid power system by quasi-oppositional harmony search algorithm. *Int. J. Electr. Power Energy Syst.* **2016**, *78*, 715–734. [CrossRef]
10. Ganguly, S.; Mahto, T.; Mukherjee, V. Integrated frequency and power control of an isolated hybrid power system considering scaling factor based fuzzy classical controller. *Swarm Evol. Comput.* **2017**, *32*, 184–201. [CrossRef]
11. Mahto, T.; Mukherjee, V. Evolutionary optimization technique for comparative analysis of different classical controllers for an isolated wind–diesel hybrid power system. *Swarm Evol. Comput.* **2016**, *26*, 120–136. [CrossRef]

12. Pandey, S.K.; Mohanty, S.R.; Kishor, N.; Catalão, J.P.S. Frequency regulation in hybrid power systems using particle swarm optimization and linear matrix inequalities based robust controller design. *Int. J. Electr. Power Energy Syst.* **2014**, *63*, 887–900. [CrossRef]
13. Mahto, T.; Malik, H.; Mukherjee, V. Fractional Order Control and Simulation of Wind-Biomass Isolated Hybrid Power System Using Particle Swarm Optimization. In *Applications of Artificial Intelligence Techniques in Engineering*; Springer: Berlin/Heidelberg, Germany, 2019; pp. 277–287. [CrossRef]
14. Mohanty, D.; Panda, S. Modified Salp Swarm Algorithm-Optimized Fractional-Order Adaptive Fuzzy PID Controller for Frequency Regulation of Hybrid Power System with Electric Vehicle. *J. Control. Autom. Electr. Syst.* **2021**, *32*, 416–438. [CrossRef]
15. Nayak, P.C.; Nayak, B.P.; Prusty, R.C.; Panda, S. Sunflower optimization based fractional order fuzzy PID controller for frequency regulation of solar-wind integrated power system with hydrogen aqua equalizer-fuel cell unit. *Energy Sources Part A Recover. Util. Environ. Eff.* **2021**, *1*, 1–19. [CrossRef]
16. Kumar, N.K.; Gandhi, V.I. Design of fuzzy logic controller for load frequency control in an isolated hybrid power system. *J. Intell. Fuzzy Syst.* **2020**, *39*, 8273–8283. [CrossRef]
17. Khadanga, R.K.; Kumar, A.; Panda, S. Frequency control in hybrid distributed power systems via type-2 fuzzy PID controller. *IET Renew. Power Gener.* **2021**, *15*, 1706–1723. [CrossRef]
18. Kumar, N.K.; Gopi, R.S.; Kuppusamy, R.; Nikolovski, S.; Teekaraman, Y.; Vairavasundaram, I.; Venkateswarulu, S. Fuzzy Logic-Based Load Frequency Control in an Island Hybrid Power System Model Using Artificial Bee Colony Optimization. *Energies* **2022**, *15*, 2199. [CrossRef]
19. Mahto, T.; Mukherjee, V. A novel scaling factor based fuzzy logic controller for frequency control of an isolated hybrid power system. *Energy* **2017**, *130*, 339–350. [CrossRef]
20. Goya, T.; Omine, E.; Kinjyo, Y.; Senjyu, T.; Yona, A.; Urasaki, N.; Funabashi, T. Frequency control in isolated island by using parallel operated battery systems applying H∞ control theory based on droop characteristics. *IET Renew. Power Gener.* **2011**, *5*, 160–166. [CrossRef]
21. Singh, V.P.; Mohanty, S.R.; Kishor, N.; Ray, P.K. Robust H-infinity load frequency control in hybrid distributed generation system. *Int. J. Electr. Power Energy Syst.* **2013**, *46*, 294–305. [CrossRef]
22. Singh, B.; Agrawal, G. Enhancement of voltage profile by incorporation of SVC in power system networks by using optimal load flow method in MATLAB/Simulink environments. *Energy Rep.* **2018**, *4*, 418–434. [CrossRef]
23. Ćalasan, M.; Konjić, T.; Kecojević, K.; Nikitović, L. Optimal Allocation of Static Var Compensators in Electric Power Systems. *Energies* **2020**, *13*, 3219. [CrossRef]
24. Najafi, S.; Abedi, M.; Hosseinian, S. A Novel Approach to Optimal Allocation of SVC using Genetic Algorithms and Continuation Power Flow. In Proceedings of the 2006 IEEE International Power and Energy Conference, Putra Jaya, Malaysia, 28–29 November 2006. [CrossRef]
25. Agarwal, P.; Baleanu, D.; Chen, Y.; Momani, S.; Machado, J.A.T. *Fractional Calculus: ICFDA 2018*; Springer: Berlin/Heidelberg, Germany, 2019.
26. Valério, D.; Machado, J.T.; Kiryakova, V. Some pioneers of the applications of fractional calculus. *Fract. Calc. Appl. Anal.* **2014**, *17*, 552–578. [CrossRef]
27. Pan, I.; Das, S. Brief Introduction to Computational Intelligence Paradigms for Fractional Calculus Researchers. In *Intelligent Fractional Order Systems and Control*; Springer: Berlin/Heidelberg, Germany, 2013; Volume 438, pp. 63–85. [CrossRef]
28. Ranganayakulu, R.; Babu, G.U.B.; Rao, A.S.; Patle, D.S. A comparative study of fractional order PIλ/PIλDμ tuning rules for stable first order plus time delay processes. *Resour.-Effic. Technol.* **2016**, *2*, S136–S152.
29. Saddique, M.S. Solution to optimal reactive power dispatch in transmission system using meta-heuristic techniques—Status and technological review. *Electr. Power Syst. Res.* **2020**, *178*, 106031. [CrossRef]
30. Arya, Y. A novel CFFOPI-FOPID controller for AGC performance enhancement of single and multi-area electric power systems. *ISA Trans.* **2019**, *100*, 126–135. [CrossRef] [PubMed]
31. Arya, Y.; Dahiya, P.; Çelik, E.; Sharma, G.; Gözde, H.; Nasiruddin, I. AGC performance amelioration in multiarea inter-connected thermal and thermal-hydro-gas power systems using a novel controller. *Eng. Sci. Technol. Int. J.* **2021**, *24*, 384–396.
32. Arya, Y. Impact of ultra-capacitor on automatic generation control of electric energy systems using an optimal FFOID controller. *Int. J. Energy Res.* **2019**, *43*, 8765–8778. [CrossRef]
33. Arya, Y. Effect of energy storage systems on automatic generation control of interconnected traditional and restructured energy systems. *Int. J. Energy Res.* **2018**, *43*, 6475–6493. [CrossRef]
34. Arya, Y. AGC of PV-thermal and hydro-thermal power systems using CES and a new multi-stage FPIDF-(1+ PI) controller. *Renew. Energy* **2019**, *134*, 796–806. [CrossRef]
35. Amoussou, I.; Tanyi, E.; Ali, A.; Agajie, T.F.; Khan, B.; Ballester, J.B.; Nsanyuy, W.B. Optimal Modeling and Feasibility Analysis of Grid-Interfaced Solar PV/Wind/Pumped Hydro Energy Storage Based Hybrid System. *Sustainability* **2023**, *15*, 1222. [CrossRef]
36. Banerjee, A.; Mukherjee, V.; Ghoshal, S.P. An opposition-based harmony search algorithm for engineering optimization problems. *Ain Shams Eng. J.* **2014**, *5*, 85–101. [CrossRef]
37. Pan, I.; Das, S. Fractional order fuzzy control of hybrid power system with renewable generation using chaotic PSO. *ISA Trans.* **2016**, *62*, 19–29. [CrossRef] [PubMed]

38. Fathy, A.; Rezk, H.; Ferahtia, S.; Ghoniem, R.M.; Alkanhel, R.; Ghoniem, M.M. A New Fractional-Order Load Frequency Control for Multi-Renewable Energy Interconnected Plants Using Skill Optimization Algorithm. *Sustainability* **2022**, *14*, 14999. [CrossRef]
39. Hailu, E.A.; Salau, A.O.; Godebo, A.J. Assessment of Solar Energy Potential of East Gojjam Zone Ethiopia Using Angestrom-Prescott Model. *Int. J. Eng. Res. Afr.* **2021**, *53*, 171–179. [CrossRef]
40. Hailu, E.A.; Godebo, A.J.; Rao, G.L.S.; Salau, A.O.; Agajie, T.F.; Awoke, Y.A.; Anteneh, T.M. Assessment of Solar Resource Potential for Photovoltaic Applications in East Gojjam Zone, Ethiopia. In *International Conference on Advances of Science and Technology*; Springer: Berlin/Heidelberg, Germany, 2020; pp. 389–403. [CrossRef]
41. Hailu, E.A.; Mezgebu, C. Design and simulation of standalone hybrid (solar/biomass) electricity generation system for a rural village in Ethiopia. *Int. J. Sci. Eng. Res.* **2017**, *8*, 1570–1574.
42. Pan, I.; Das, S. Fractional Order AGC for Distributed Energy Resources Using Robust Optimization. *IEEE Trans. Smart Grid.* **2015**, *7*, 2175–2186. [CrossRef]
43. Latif, A.; Hussain, S.S.; Das, D.C.; Ustun, T.S.; Iqbal, A. A review on fractional order (FO) controllers' optimization for load frequency stabilization in power networks. *Energy Rep.* **2021**, *7*, 4009–4021. [CrossRef]
44. Mahto, T.; Malik, H.; Mukherjee, V.; Alotaibi, M.A.; Almutairi, A. Renewable generation based hybrid power system control using fractional order-fuzzy controller. *Energy Rep.* **2021**, *7*, 641–653. [CrossRef]
45. Padhy, S.; Panda, S. Application of a simplified Grey Wolf optimization technique for adaptive fuzzy PID controller design for frequency regulation of a distributed power generation system. *Prot. Control. Mod. Power Syst.* **2021**, *6*, 1–16. [CrossRef]
46. Das, S.; Pan, I.; Das, S.; Gupta, A. A novel fractional order fuzzy PID controller and its optimal time domain tuning based on integral performance indices. *Eng. Appl. Artif. Intell.* **2012**, *25*, 430–442. [CrossRef]
47. Barik, A.K.; Das, D.C. Expeditious frequency control of solar photovoltaic/biogas/biodiesel generator based isolated renewable microgrid using grasshopper optimisation algorithm. *IET Renew. Power Gener.* **2018**, *12*, 1659–1667. [CrossRef]
48. Coban, H.H.; Rehman, A.; Mousa, M. Load Frequency Control of Microgrid System by Battery and Pumped-Hydro Energy Storage. *Water* **2022**, *14*, 1818. [CrossRef]
49. Salama, H.S.; Kotb, K.M.; Vokony, I.; Dán, A. The Role of Hybrid Battery–SMES Energy Storage in Enriching the Permanence of PV–Wind DC Microgrids: A Case Study. *Eng* **2022**, *3*, 207–223. [CrossRef]
50. Das, S.; Pan, I.; Das, S. Fractional order fuzzy control of nuclear reactor power with thermal-hydraulic effects in the presence of random network induced delay and sensor noise having long range dependence. *Energy Convers. Manag.* **2013**, *68*, 200–218. [CrossRef]
51. Das, S.; Pan, I.; Das, S. Performance comparison of optimal fractional order hybrid fuzzy PID controllers for handling oscillatory fractional order processes with dead time. *ISA Trans.* **2013**, *52*, 550–566. [CrossRef] [PubMed]
52. Pan, I.; Korre, A.; Das, S.; Durucan, S. Chaos suppression in a fractional order financial system using intelligent re-grouping PSO based fractional fuzzy control policy in the presence of fractional Gaussian noise. *Nonlinear Dyn.* **2012**, *70*, 2445–2461. [CrossRef]
53. Rentería-Baltiérrez, F.Y.; Reyes-Melo, M.E.; Puente-Córdova, J.G.; López-Walle, B. Application of fractional calculus in the mechanical and dielectric correlation model of hybrid polymer films with different average molecular weight matrices. *Polym. Bull.* **2022**, *1*, 1–21. [CrossRef]
54. Viola, J.; Chen, Y. A Fractional-Order On-Line Self Optimizing Control Framework and a Benchmark Control System Accelerated Using Fractional-Order Stochasticity. *Fractal Fract.* **2022**, *6*, 549. [CrossRef]
55. Biswal, K.; Swain, S.; Tripathy, M.C.; Kar, S.K. Modeling and Performance Improvement of Fractional-Order Band-Pass Filter Using Fractional Elements. *IETE J. Res.* **2021**, *1*, 1–10. [CrossRef]
56. Babes, B.; Albalawi, F.; Hamouda, N.; Kahla, S.; Ghoneim, S.S. Fractional-fuzzy PID control approach of photovoltaic-wire feeder system (PV-WFS): Simulation and HIL-based experimental investigation. *IEEE Access* **2021**, *9*, 159933–159954. [CrossRef]
57. Sahoo, D.K.; Sahu, R.K.; Panda, S. Chaotic Harris hawks optimization based type-2 fractional order fuzzy PID controller for frequency regulation of power systems. *Int. J. Ambient Energy* **2022**, *43*, 3832–3844. [CrossRef]
58. Kullapadayachi, S.G.; Sivalingam, R. Design, analysis, and real-time validation of type-2 fractional order fuzzy PID controller for energy storage–based microgrid frequency regulation. *Int. Trans. Electr. Energy Syst.* **2021**, *31*, e12766. [CrossRef]
59. Das, S.; Datta, S.; Saikia, L.C. Load frequency control of am ulti-source multi-area thermal system including biogas–solar thermal along with pumped hydro energy storage system using MBA-optimized 3DOF-TIDN controller. *Int. Trans. Electr. Energy Syst.* **2021**, *31*, e13165. [CrossRef]
60. Jain, N.; Parmar, G.; Gupta, R.; Khanam, I. Performance evaluation of GWO/PID approach in control of ball hoop system with different objective functions and perturbation. *Cogent Eng.* **2018**, *5*, 1465328. [CrossRef]
61. Alamri, H.S.; A Alsariera, Y.; Zamli, K.Z. Opposition-Based Whale Optimization Algorithm. *Adv. Sci. Lett.* **2018**, *24*, 7461–7464. [CrossRef]
62. Liu, X. Optimization design on fractional order PID controller based on adaptive particle swarm optimization algorithm. *Nonlinear Dyn.* **2015**, *84*, 379–386. [CrossRef]
63. Shiva, C.K.; Mukherjee, V. Design and analysis of multi-source multi-area deregulated power system for automatic generation control using quasi-oppositional harmony search algorithm. *Int. J. Electr. Power Energy Syst.* **2016**, *80*, 382–395. [CrossRef]
64. Shankar, G.; Mukherjee, V. Quasi oppositional harmony search algorithm based controller tuning for load frequency control of multi-source multi-area power system. *Int. J. Electr. Power Energy Syst.* **2016**, *75*, 289–302. [CrossRef]

65. Kumar, A.; Shankar, G. Quasi-oppositional harmony search algorithm based optimal dynamic load frequency control of a hybrid tidal–diesel power generation system. *IET Gener. Transm. Distrib.* **2018**, *12*, 1099–1108. [CrossRef]
66. Shiva, C.K.; Shankar, G.; Mukherjee, V. Automatic generation control of power system using a novel quasi-oppositional harmony search algorithm. *Int. J. Electr. Power Energy Syst.* **2015**, *73*, 787–804. [CrossRef]
67. Mohanty, P.; Sahu, R.K.; Sahoo, D.K.; Panda, S. Adaptive differential evolution and pattern search tuned fractional order fuzzy PID for frequency control of power systems. *Int. J. Model. Simul.* **2022**, *42*, 240–254. [CrossRef]
68. Annamraju, A.; Nandiraju, S. Robust frequency control in a renewable penetrated power system: An adaptive fractional order-fuzzy approach. *Prot. Control. Mod. Power Syst.* **2019**, *4*, 1–15. [CrossRef]
69. Mahto, T.; Malik, H.; Bin Arif, M.S. Load frequency control of a solar-diesel based isolated hybrid power system by fractional order control using partial swarm optimization. *J. Intell. Fuzzy Syst.* **2018**, *35*, 5055–5061. [CrossRef]